OPEN ACCESS
IOP Publishing
Superconductor Science and Technology
Supercond. Sci. Technol. **33** (2020) 044003 (11pp)
https://doi.org/10.1088/1361-6668/ab7297

Numerical simulation of flux jump behavior in REBaCuO ring bulks with an inhomogeneous J_c profile during pulsed-field magnetization

Tatsuya Hirano[1,3], Hiroyuki Fujishiro[1], Tomoyuki Naito[1] and Mark D Ainslie[2]

[1] Department of Physical Science and Materials Engineering, Faculty of Science and Engineering, Iwate University, 4-3-5 Ueda, Morioka 020-8551, Japan
[2] Bulk Superconductivity Group, Department of Engineering, University of Cambridge, Trumpington Street, Cambridge CB2 1PZ, United Kingdom

E-mail: g0318132@iwate-u.ac.jp

Received 27 September 2019, revised 5 January 2020
Accepted for publication 3 February 2020
Published 17 February 2020

Abstract

We have investigated the electromagnetic and thermal properties of a REBaCuO ring bulk with an inhomogeneous critical current density, J_c, profile during pulsed field magnetization (PFM) using a numerical simulation and compared those to a bulk with a homogeneous J_c profile. A notch was introduced in the bulk periphery, which was assumed as a crack existing in the actual bulk material. A sudden flux penetration (flux jump) took place through the notch area and as a result, a large temperature rise also took place around this notch. Consequently, the final trapped field profile was simulated to be a 'C-shaped profile', which qualitatively reproduced our previous experimental results. The size and position dependences of the notch on the flux penetration behaviour were also simulated, in which a larger and outer notch promotes the flux jump phenomenon easily. On the other hand, in the homogeneous model, under the same conditions, no flux jump phenomenon was observed. These results suggest that the imperfection in the bulk can be a possible starting point of the flux jump. The electromagnetic and thermal hoop stresses were also simulated in the ring bulk during PFM, in which the electromagnetic stress and the thermal stress were both observed to be lower than the fracture strength of the bulk material. This provides good evidence that the experimentally observed 'C-shaped profile' results from the flux jump rather than the fracture of the bulk.

Keywords: bulk superconductor, pulsed field magnetization, flux jump, mechanical stress, numerical simulation, inhomogeneous Jc profile

(Some figures may appear in colour only in the online journal)

1. Introduction

REBaCuO (RE: rare earth element or Y) superconducting bulks can be used as strong trapped field magnets (TFMs), which have generated magnetic fields of over 17 T to date [1–3]. Such TFMs have been used for practical applications such as a compact cryogen-free nuclear magnetic resonance (NMR) spectrometer, magnetic separation, magnetic drug

[3] Author to whom any correspondence should be addressed.

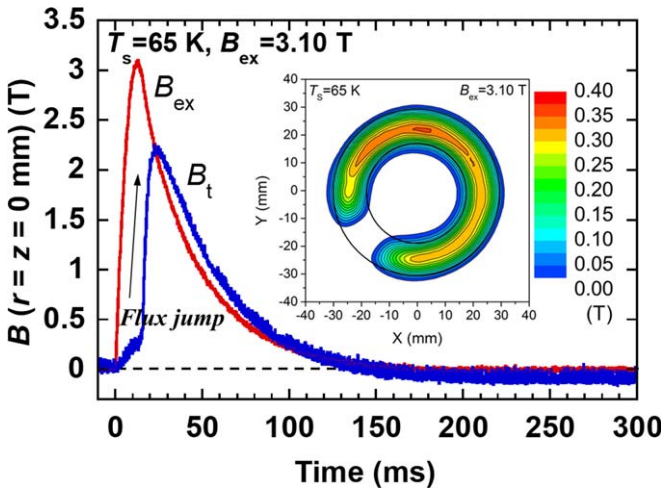

Figure 1. Time evolution of the trapped field, $B_t(t)$, at the center of the ring bulk ($r = z = 0$ mm) and the applied field, $B_{ex}(t)$, for $B_{ex} = 3.10$ T at 65 K. The inset shows the trapped field profile mapped 1.0 mm above the bulk surface, in which the contour of the ring bulk is also shown. © 2016 IEEE. Reprinted, with permission, from [21].

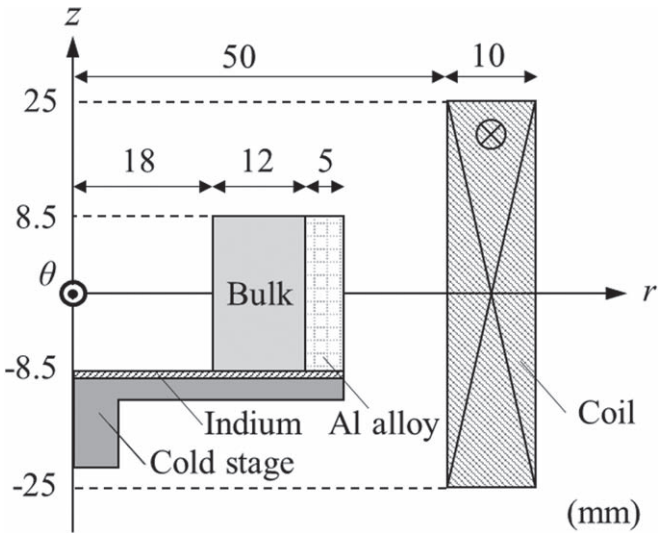

Figure 2. 2D cross-section of the numerical model of the ring bulk and magnetizing coil for pulsed-field magnetization.

delivery systems and rotating machines [4–8]. Today, state-of-the-art bulk materials have potential to trap magnetic field of over 20 T at low temperatures from the viewpoint of magnetic field and temperature dependence of the critical current density, $J_c(B, T)$. However, REBaCuO TFMs suffer from mechanical fracture of the brittle ceramic material due to a large Lorentz force, $\boldsymbol{F} = \boldsymbol{J} \times \boldsymbol{B}$, ($\boldsymbol{J}$ is the current density and $\boldsymbol{B}$ is the magnetic field), that is developed during field-cooled magnetization (FCM) in high applied magnetic fields [9–12]. We have investigated the mechanical properties of disk- and ring-shaped REBaCuO bulks during FCM using numerical simulations based on the finite element method (FEM), and proposed optimal reinforcement structures made of metal to prevent mechanical fracture [13–17]. The mechanical properties have also been investigated analytically for bulks with an infinite height during FCM and zero-field-cooled magnetization (ZFCM) [18–20]. However, looking towards industrial applications, the pulsed field magnetization (PFM) is the most practical technique to magnetize superconducting bulks because of the inexpensive and mobile experimental setup in contrast to FCM/ZFCM.

In our previous study [21], we performed PFM experiments on a GdBaCuO ring bulk. Figure 1 shows the results of time evolution of the trapped field, $B_t(t)$, at the center of the ring bulk and the applied field, $B_{ex}(t)$, for $B_{ex} = 3.10$ T at 65 K. The final trapped field of the center of the ring bulk was a negative value after PFM and exhibited a 'C-shaped' trapped field profile, as shown in the inset of figure 1. We concluded, in this work, that these results may come from the bulk fracture: the ring bulk was reinforced only by an outer metal ring, which was effective for the tensile stress during the descending stage of PFM, but not effective for the compressive stress during the ascending stage. In addition, at that time, we had not yet developed a simulation technique to investigate mechanical properties precisely. The flux jump behaviour in the ring-shaped bulk was also observed experimentally during PFM [22, 23].

During the magnetizing process of REBaCuO superconducting bulks, a flux jump sometimes occurs, which usually causes a locally large temperature rise and reduces the final trapped field, especially during FCM. However, a flux jump, which was named a 'giant flux leap' by Weinstein *et al* [24], enables the magnetic flux to penetrate the bulk more easily in the ascending process of PFM and can enhance the final trapped field [24–27]. Recently several authors have reported the numerical simulation of the flux jump phenomena during the PFM process [27–29]. However, the influence of the flux jump and the resultant large temperature rise on mechanical fracture during PFM has not been well clarified yet.

In this study, we reconsider the cause of the reported 'C-shaped profile' and perform numerical simulation of the PFM process for a realistic REBaCuO ring bulk. The flux jump phenomenon and mechanical stress behavior were simulated for ring bulks with homogeneous and inhomogeneous J_c profiles. We discuss the mechanical stresses in such a realistic REBaCuO ring bulk during PFM to clarify the risk of fracture for the bulk. This study contributes to the development of ring-shaped TFMs from the viewpoints of the electromagnetic, thermal and stress behaviors during PFM.

2. Numerical simulation framework

Based on our experimental setup for PFM [21], we constructed a three-dimensional (3D) model for a REBaCuO ring bulk (60 mm in outer diameter (O.D.), 36 mm in inner diameter (I.D.) and 17 mm in height (H)), which was the same size as the previous study. Figure 2 shows the two-dimensional (2D) cross-section of the 3D numerical model. The ring bulk was mounted in an Al alloy ring holder 5 mm in width (70 mm in O.D. and 60 mm in I.D.) with the same

Table 1. Numerical parameters for the J_c (B, T) characteristics in equation (1) at 65, 70, 75 and 80 K used in the numerical simulation.

T (K)	J_{c1} (Am^{-2})	B_L (T)	J_{c2} (Am^{-2})	B_{max} (T)	k
65	1.0×10^9	0.46	5.9×10^8	2.4	1.1
70	7.9×10^8	0.40	3.8×10^8	2.2	1.3
75	6.1×10^8	0.32	2.2×10^8	1.8	1.8
80	4.3×10^8	0.21	1.1×10^8	0.65	2.8

height as the bulk. The Al alloy is a suitable material for the reinforcement of the ring bulk for NMR apparatus because it is non-magnetic and has a higher mechanical strength, compared to pure aluminum. The bulk was cooled to $T_s = 65$ K from the bottom surface attached to the cold stage using a thin indium sheet and was magnetized by PFM using an outer magnetizing coil (120 mm in O.D., 100 mm in I.D. and 50 mm in H). Single magnetic pulses with a rise time of 13 ms, a duration of 200 ms, and amplitudes ranging from $B_{ex} = 2.53$ to 4.0 T, were applied to the bulk via a pulsed current in the coil. During the PFM process ($t = 1 \sim 300$ ms), the time evolution of the trapped magnetic field, $B_t(t)$, was monitored at the center of ring bulk ($r = z = 0$ mm). After the PFM process ($t = 7000$ ms) at the steady state without flux flow, the B_t distribution was also mapped 0 mm ($z = 8.5$ mm) or 1.0 mm ($z = 9.5$ mm) above the bulk surface. Physical phenomena during PFM are described by the fundamental electromagnetic and thermal equations in [30]. The power-n law ($n = 20$) was used to describe the highly nonlinear E-J characteristic of the bulk material [31]. The following magnetic field and temperature dependence of critical current density, $J_c(B, T)$, proposed by Jirsa *et al* [32], was used in the simulation.

$$J_c(B,\ T) = J_{c1}(T)\exp\left(-\frac{B}{B_L(T)}\right) + J_{c2}(T)\frac{B}{B_{max}(T)} \times \exp\left[\frac{1}{k(T)}\left(1 - \left(\frac{B}{B_{max}(T)}\right)^{k(T)}\right)\right], \quad (1)$$

where the parameters (J_{c1}, B_L, J_{c2}, B_{max} and k) for the $J_c(B)$ at each temperature are shown in table 1. Figure 3 shows the $J_c(B, T)$ profiles used in the simulation, compared with $J_c(B, T)$ of the GdBaCuO bulk measured using SQUID magnetometer, which has typical characteristics in the recent bulk material [33]. The similar experimental $J_c(B, T)$ were also reported [34]. The $J_c(B, T)$ characteristics used in this simulation were slightly modified from the SQUID data [33] to reproduce the experimental $B_t(t)$ profile shown in figure 3. The temperature dependences of $J_c(B, T)$ were linearly interpolated to simulate the results during PFM, as described in [35]. The REBaCuO ring bulk are assumed to be isotropic and homogeneous for simplicity. The commercial software package, Photo-Eddy, combined with Photo-Thermo and Photo-Elas (Photon Ltd, Japan), was used for analyses of electromagnetic, thermal and mechanical properties. The anisotropic thermal conductivities $\kappa_{ab} = 20$ Wm^{-1}K^{-1} in the ab-plane and $\kappa_c = 4$ Wm^{-1}K^{-1} along the c-axis of

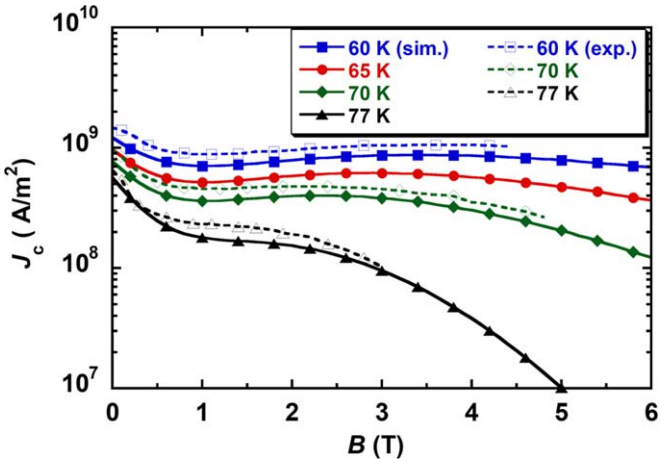

Figure 3. Magnetic field and temperature dependences of the critical current density, $J_c(B, T)$, between 60 K and 77 K used in the simulation. The $J_c(B, T)$ profiles of GdBaCuO bulk measured using SQUID magnetometer are also shown in comparison [33].

Table 2. Mechanical parameters of the REBaCuO bulk and Al alloy used in the numerical simulation.

	E (GPa)	ν	α_0 (K^{-1})
REBaCuO bulk	100	0.33	5.20×10^{-6}
Al alloy	78	0.34	1.48×10^{-5}

(E: Young's modulus, ν: Poisson ratio, α_0: thermal expansion coefficient).

REBaCuO bulk were assumed to be independent of temperature. The temperature-dependent specific heat, C, of the bulk was used [34]. The simulation procedure of electromagnetic and thermal properties are described elsewhere in detail [30]. The elastic behaviour of an isotropic material can be explained by Hooke's law, in which the stress is linearly proportional to the strain [13]. The electromagnetic hoop stress, σ_θ^{EM}, and the thermal hoop stress, σ_θ^{therm}, during PFM were calculated for each case. Table 2 summarizes the mechanical parameters (Young's modulus, E, Poisson ratio, ν, and thermal expansion coefficient, α_0) of the REBaCuO bulk and the Al alloy used in the simulation.

In this study, homogeneous and inhomogeneous models are constructed for the J_c distribution, as shown in figures 4(a) and (b). The same model was used for the electromagnetic, thermal, and mechanical simulations, which was equally divided into 36 elements along the circumferential (θ) direction. Along the z- and r-directions, the bulk region was divided by a 0.5 mm mesh and the other region was divided by a 1.0 mm mesh. The total number of mesh elements was 227 304. The computational time needed to solve all the electromagnetic, thermal, and mechanical models for one condition (T_s, B_{ex}) was approximately about 6 h. In the inhomogeneous model, a notch (2 mm in width, 17 mm in H and 1 element along the θ-direction) is placed at the bulk periphery ($r = 28$–30 mm) as a non-superconducting material with very low thermal conductivity ($\kappa = 1 \times 10^{-8}$ Wm^{-1}K^{-1}) and specific heat ($C = 1 \times 10^{-8}$ Jkg^{-1}K^{-1}). The

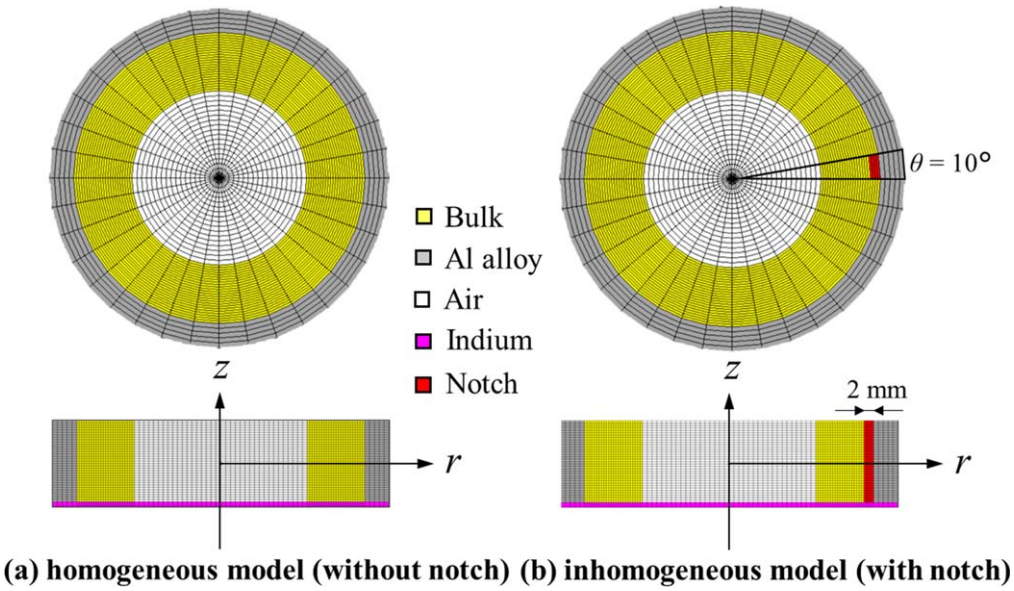

Figure 4. Schematic view of the numerical models for the ring-shaped bulk: (a) homogeneous model (without notch), (b) inhomogeneous model (with notch) (*see text*).

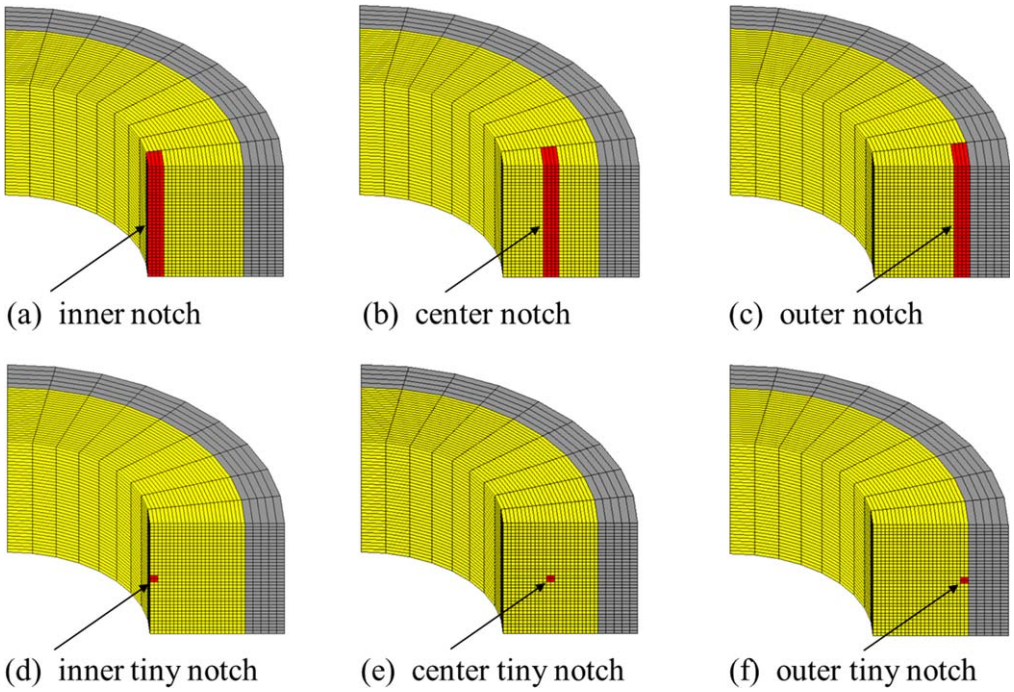

Figure 5. Schematic view of the numerical models for the ring-shaped bulk with various notches: (a) inner notch, (b) center notch, (c) outer notch, (d) inner tiny notch, (e) center tiny notch and (f) outer tiny notch (*see text*).

boundary condition between the notch region and bulk region (or outer air region) is not adiabatic, but heat conductive.

The size of the notch shown in figure 4 is much larger than that of a realistic crack. To clarify the influence of notch size and position on the flux jump, the inhomogeneous models with various types of notches are also constructed. The models with the notch (2.0 mm in width, 17 mm in H and 1 element along the θ-direction) at $r = 18$, 23, 28 mm are denoted as 'inner notch', 'center notch' and 'outer notch', respectively, as shown in figures 5(a)–(c). Note that the 'outer notch' is the same as that shown in figure 4. In addition, the models with a tiny notch (1.0 mm in width, 1.0 mm in H and 1 element along the θ-direction) at $r = 18$, 23, 28 mm are denoted as 'inner tiny notch', 'center tiny notch' and 'outer tiny notch', respectively, as shown in figures 5(d)–(f).

Since a flux jump is a thermomagnetic instability, the numerical simulation of the flux jump is sensitive to the mesh sizes, the initial and boundary conditions, and so on. However, this study presents the qualitative tendency of the flux jump behavior based on the chosen mesh.

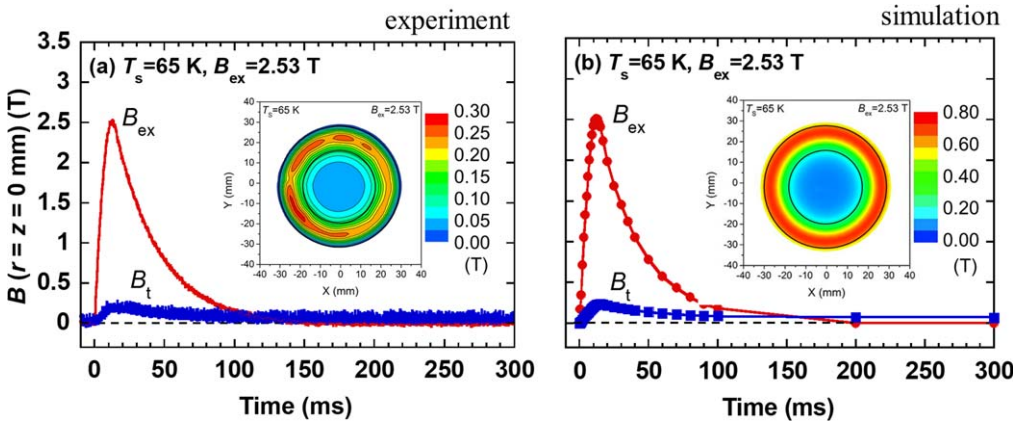

Figure 6. (a) Experimental (© 2016 IEEE. Reprinted, with permission, from [21]) and (b) present simulation results of time evolution of the trapped field, $B_t(t)$, at the center of the ring bulk ($r = z = 0$ mm) and applied pulsed field, $B_{ex}(t)$, for $B_{ex} = 3.10$ T at 65 K. The inset of each figure shows the trapped field profile mapped 1.0 mm above the bulk surface ($z = 9.5$ mm). The contour of the ring bulk is shown in the inset of each figure.

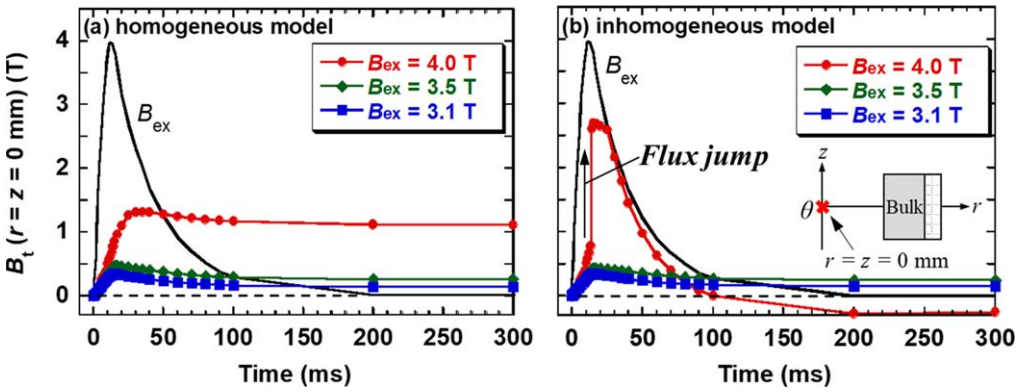

Figure 7. Time evolution of the trapped field, B_t, at the center of the ring bulk ($r = z = 0$ mm) for $B_{ex} = 3.1\sim4.0$ T at $T_s = 65$ K and applied pulsed field, $B_{ex}(t)$, for $B_{ex} = 4.0$ T using (a) the homogeneous model and (b) the inhomogeneous model.

3. Numerical simulation results and discussion

3.1. Verification of simulation results

To verify the accuracy of numerical simulation, the numerical results are compared to the previous experimental results. Figures 6(a) and (b), respectively, show the experimental results by Mochizuki *et al* [21] and the present simulation results using the homogenous model, in which the time evolution of the trapped field, $B_t(t)$, at the center of the ring bulk ($r = z = 0$ mm) and applied pulsed field, $B_{ex}(t)$, for $B_{ex} = 2.53$ T at 65 K are shown. The inset in each figure shows the trapped field profile mapped 1.0 mm above the bulk surface ($z = 9.5$ mm), in which the contour of the ring bulk is also shown. The experimental $B_t(t)$ behavior at the center of the ring bulk was reproduced by numerical simulation well, in which the fitting parameters for equation (1) are adjusted to adequately reproduce the maximum B_t value during PFM process. However, the B_t value at the surface of the bulk periphery in the simulation is about 2.5 times higher than that in the experiment. The difference in the B_t value may come from the ideally homogenous $J_c(B, T)$ characteristics in the simulation model, assuming no position dependence of J_c. Furthermore, in the experiment, the magnetic flux might penetrate into the actual bulk easily from a lower J_c region and the final trapped field becomes lower [36].

3.2. Comparison of simulation results between homogeneous and inhomogeneous models

Figure 7(a) shows time evolution of the trapped field, $B_t(t)$, at the center of the ring bulk ($r = z = 0$ mm) for $B_{ex} = 3.1\sim4.0$ T at $T_s = 65$ K using the homogeneous model. For an applied field of $B_{ex} = 3.1$ T, $B_t(t)$ took a peak value and then decreased to small B_t value at $t = 300$ ms, at which the magnetic flux cannot penetrate well to the center of the bulk due to its magnetic shielding. The final B_t value increased with increasing B_{ex}. For $B_{ex} = 3.1\sim4.0$ T, no flux jump took place. Figure 7(b) shows similar results using the inhomogeneous model, as shown in figure 4(b). The time evolution of $B_t(t)$ for B_{ex} lower than 3.5 T was similar to those using the homogeneous model. However, the flux jump took place for $B_{ex} = 4.0$ T, for which $B_t(t)$ increased rapidly at 14 ms and reached its peak value of $B_t = 2.7$ T at $t = 15$ ms. In the descending stage, $B_t(t)$ decreased gradually with increasing time and eventually reached a negative value of $B_t = -0.3$ T, which is a clear evidence of the disturbance of the circulating

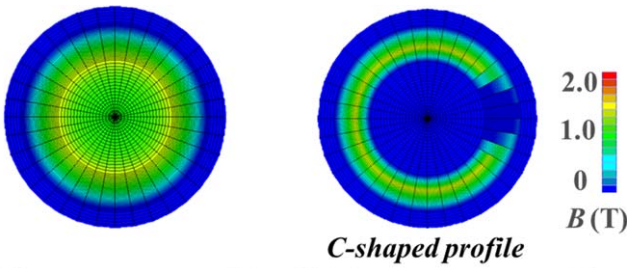

Figure 8. Final trapped field distributions on the bulk surface ($z = 9.5$ mm) for $B_{ex} = 4.0$ T at 65 K; (a) homogeneous model, (b) inhomogeneous model.

supercurrent. The $B_t(t)$ behavior qualitatively reproduced experimental results, as shown in figure 1, only in the inhomogeneous model.

Figures 8(a) and (b), respectively, show final trapped field distributions on the bulk surface ($z = 9.5$ mm) for $B_{ex} = 4.0$ T at 65 K using the homogeneous and inhomogeneous models. In the homogeneous model, the magnetic flux was trapped symmetrically across the whole bulk and the B_t value at the center of the ring bulk was positive. On the other hand, in the inhomogeneous model, no magnetic flux was trapped at the notch area. As a result, the final B_t profile exhibited the 'C-shaped profile', which is similar to the experimental one, as shown in the inset of figure 1. In this way, the 'C-shaped profile' was reproduced only using the inhomogeneous model.

3.3. Flux dynamics and thermal behavior in the inhomogeneous model

To clarify the cause of the 'C-shaped profile' in the inhomogeneous model, the flux dynamics and thermal behavior were investigated. Figure 9(a) shows 1/4 of the top view of the numerical model, in which the notch is contained in the periphery. Figure 9(b) shows the time evolution of the trapped field, $B_t(t)$, at the center of the bulk surface ($r = 0$ mm, $z = 8.5$ mm) and applied pulsed field, $B_{ex}(t)$, for $B_{ex} = 4.0$ T at 65 K. The right vertical axis shows the time evolution of the temperature, $T(t)$, at the notch surface ($r = 28$ mm, $z = 8.5$ mm). The B_t value increased rapidly, reached a peak value of 2.7 T at $t = 20$ ms, and then gradually decreased with increasing time. A negative B_t value can be observed, even at the center of the bulk surface, similar to that at the center of the ring bulk ($r = z = 0$ mm), as shown in figure 7(b). The temperature rise at the notch surface increased significantly with increasing B_{ex}, reached around 90 K at $t = 40$ ms, and remained up to $t = 300$ ms due to the extremely low heat diffusion for the ceramic material.

Figure 9(c) shows the time evolution of the trapped field (the color of $B_t = 2$ T includes over 2 T) and temperature distributions on the bulk surface ($z = 8.5$ mm) during the ascending stage of PFM ($0\text{ ms} < t \leqslant 20\text{ ms}$). At $t \leqslant 5$ ms, the magnetic flux was concentrated mainly around the notch area, where the B_t value at the center of the bulk was nearly zero. At the same time, the temperature rise increased locally, mainly in the area of flux penetration. At $5\text{ ms} < t < 20\text{ ms}$, the magnetic flux suddenly penetrated into the notch area via a flux jump and the temperature rise gradually increased across the whole bulk region. At $t = 20$ ms, the magnetic flux completely penetrates into the center of the ring bulk and the temperature at the notch area reached around 90 K. These results in the ascending stage are reasonably understood by the following positive cycle of the flux penetration and the resultant temperature rise by the flux jump: (1) the notch area in the bulk periphery weakens the magnetic shielding effect and the magnetic flux is concentrated; (2) the flux concentration promotes a temperature rise due to the flux movement, compared to other areas; (3) the shielding effect is further decreased due to the temperature rise; and (4) the flux penetration and the resultant temperature rise are promoted more and more. This cycle leads to the flux jump in the ascending process.

Figure 9(d) shows the time evolution of the trapped field (the color of $B_t = 0$ T includes the negative value) and temperature distributions on the bulk surface ($z = 8.5$ mm) during the descending stage ($20\text{ ms} < t \leqslant 300\text{ ms}$). The magnetic flux escapes mainly from the notch area and the amount of magnetic flux decreases with increasing time. The temperature around the notch area remains as high as 90 K even at $t = 300$ ms because the thermal diffusivity is much lower, compared with the flux movement. As a result, the B_t profile exhibited the 'C-shaped profile'. The local and large temperature rise promotes a large flux flow and then leads to the 'C-shaped profile' in the trapped field. It should be noted that no flux jump takes place in the ideal homogeneous bulk in this simulation. We found that there was only a slight difference in the temperature distributions along the z-direction in the inhomogeneous model. In the actual bulks, a large number of voids, cracks and secondary phases (RE211 and Ag etc) exist. The present simulation results strongly suggest that such inhomogeneity in the bulk can trigger the flux jump easily.

3.4. The influence of notch size and position on the flux jump

To clarify the influence of the notch size and position on the flux jump, the flux dynamics and thermal behavior were investigated during PFM using the inhomogeneous models. Figure 10(a) shows the typical time evolution of the trapped field, $B_t(t)$, at the center of the ring bulk ($r = z = 0$ mm) for $B_{ex} = 3.1 \sim 4.0$ T at $T_s = 65$ K using the inhomogeneous model with the 'inner notch', as shown in figure 5. The time evolution of $B_t(t)$ for B_{ex} lower than 3.5 T was similar to those using the inhomogeneous model with the 'outer notch', as shown in figure 7(b). However, the flux jump took place for $B_{ex} = 4.0$ T and the trapped field reached its peak value of $B_t = 2.6$ T at $t = 25$ ms. The peak time becomes delayed in the case of the 'inner notch', compared with the 'outer notch'. In the descending stage, $B_t(t)$ decreased gradually with increasing time and eventually reached a negative value of $B_t = -0.1$ T.

Figure 10(b) shows the time evolution of the trapped field, $B_t(t)$, at the center of the ring bulk ($r = z = 0$ mm) for

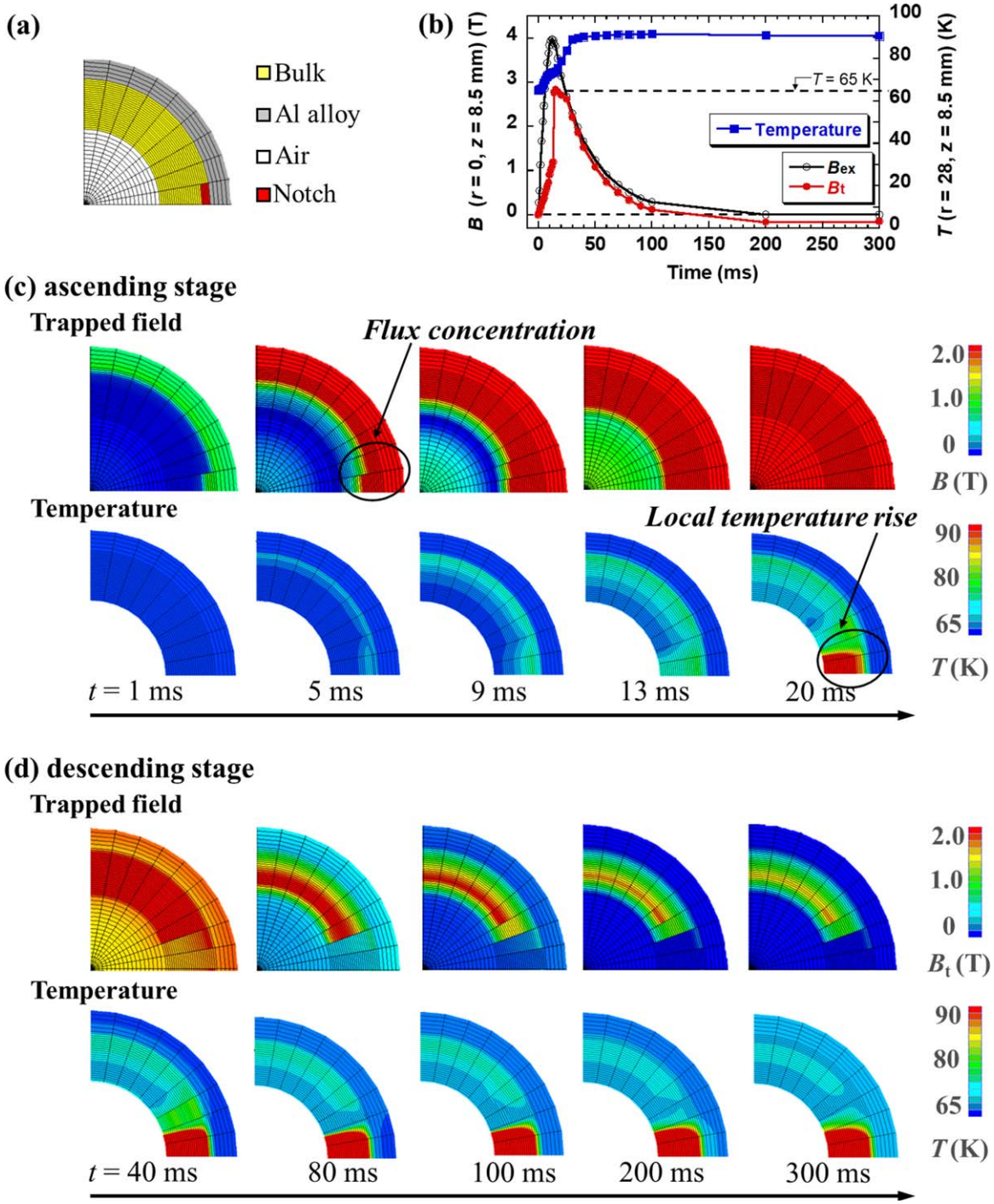

Figure 9. (a) 1/4 of the top view of the inhomogeneous model, containing the notch area. (b) Time evolution of the trapped field, $B_t(t)$, at the center of the bulk surface ($r = 0$ mm, $z = 8.5$ mm), applied pulsed field, $B_{ex}(t)$, for $B_{ex} = 4.0$ T at 65 K and temperature (right vertical axis), $T(t)$, on the notch surface ($r = 28$ mm, $z = 8.5$ mm) in the inhomogeneous model. Time evolution of the trapped field and temperature distributions on the bulk surface ($z = 8.5$ mm) in (c) the ascending stage ($t = 1\sim20$ ms) and (d) the descending stage ($t = 40\sim300$ ms) of the PFM process.

$B_{ex} = 4.0\sim5.0$ T at $T_s = 65$ K using the inhomogeneous model with the 'outer tiny notch'. The B_t value for B_{ex} lower than 4.5 T increases with increasing B_{ex}. These results are in contrast to the 'outer notch' shown in figure 7(b). These results suggest that it is more difficult for the magnetic flux to penetrate for the smaller notch. However, for $B_{ex} = 5.0$ T, a flux jump occurred, where the larger magnetic field abruptly penetrated into the bulk center, and reached its peak value of $B_t = 4.0$ T at $t = 17$ ms. The peak time becomes delayed for the 'outer tiny notch', compared with the 'outer notch'. In the descending stage, $B_t(t)$ decreased drastically with increasing time and eventually reached a small value of $B_t = 0.3$ T. Although the B_t value at the bulk center was not a negative value, the final trapped field profile exhibited the 'C-shaped

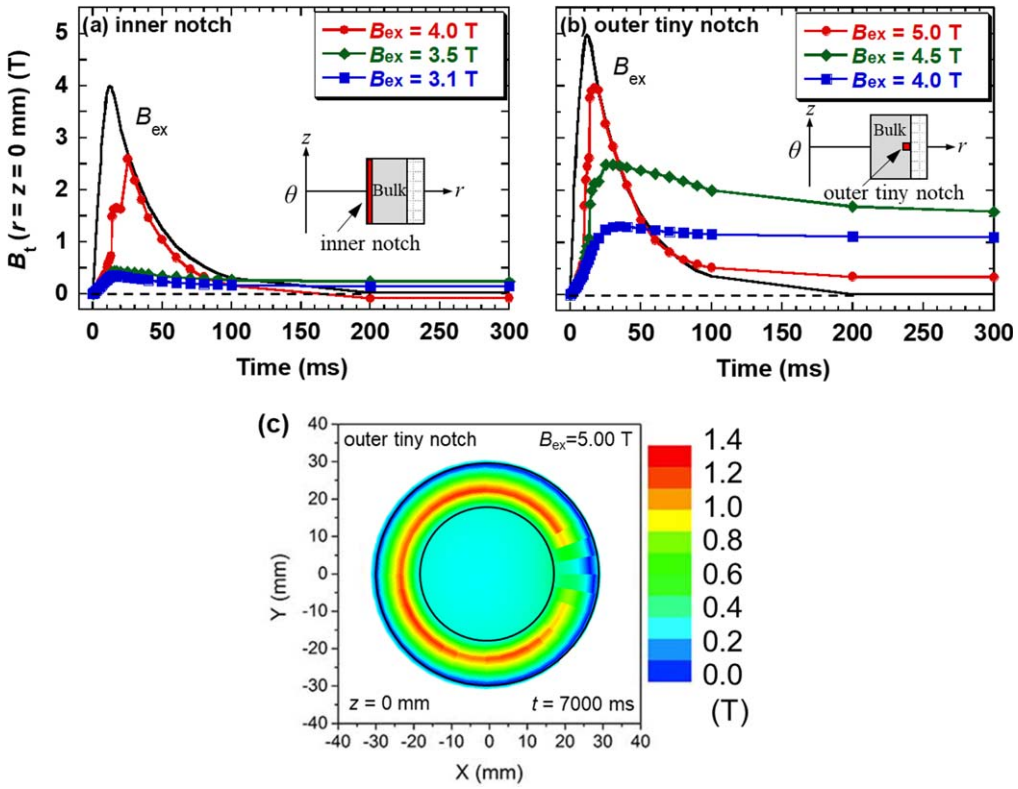

Figure 10. (a) Time evolution of the trapped field, B_t, at the center of the ring bulk ($r = z = 0$ mm) for $B_{ex} = 3.1 \sim 4.0$ T at $T_s = 65$ K and applied pulsed field, $B_{ex}(t)$, for $B_{ex} = 4.0$ T using the inhomogeneous model with the 'inner notch'. (b) Time evolution of the trapped field, B_t, at the center of the ring bulk ($r = z = 0$ mm) for $B_{ex} = 4.0 \sim 5.0$ T at $T_s = 65$ K and applied pulsed field, $B_{ex}(t)$, for $B_{ex} = 5.0$ T using the inhomogeneous model with the 'outer tiny notch'. (c) Final trapped field distributions on the bulk surface ($z = 0$ mm) for $B_{ex} = 5.0$ T at $T_s = 65$ K using the inhomogeneous model with the 'outer tiny notch'. The contour of the ring bulk is shown in the inset of figure.

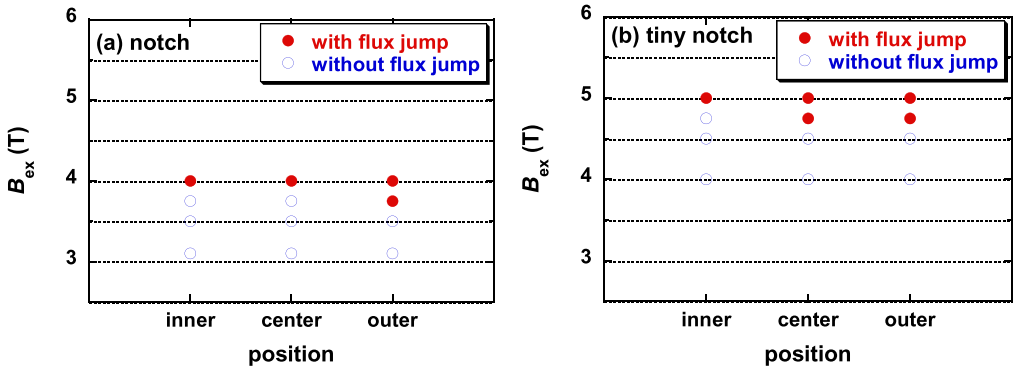

Figure 11. The mapping of the occurrence of the flux jump for (a) the inner notch, center notch and outer notch shown in figures 5(a)–(c) at $T_s = 65$ K. The mapping of the occurrence of the flux jump for (b) the inner tiny notch, center tiny notch and outer tiny notch shown in figures 5(d)–(f) at $T_s = 65$ K.

profile', as shown in figure 10(c), because of the incomplete circulating supercurrent. These results indicate that the flux jump took place even in the case of the 'outer tiny notch'.

To understand the role of notch triggering the flux jump, the critical applied field was defined as the value at which the flux jump takes place, for the inhomogeneous models with notches of various sizes and positions, during PFM. Figure 11(a) shows the mapping of the occurrence of the flux jump for the inner, center and outer notches shown in figures 5(a)–(c). The critical applied field for the flux jump was 4.0, 4.0 and 3.75 T for the inner notch, center notch and outer notch, respectively. These results suggest that a defect existing at outer side is easier to trigger a flux jump. Figure 11(b) shows the mapping of the occurrence of the flux jump for the inner tiny notch, center tiny notch and outer tiny notch shown in figures 5(d)–(f). The critical applied field for the flux jump was 5.0, 5.0 and 4.75 T for the inner, center and outer tiny notch, respectively, which was larger than that for the larger notches. These results suggest that a large applied field is necessary to cause a flux jump in the bulk with smaller

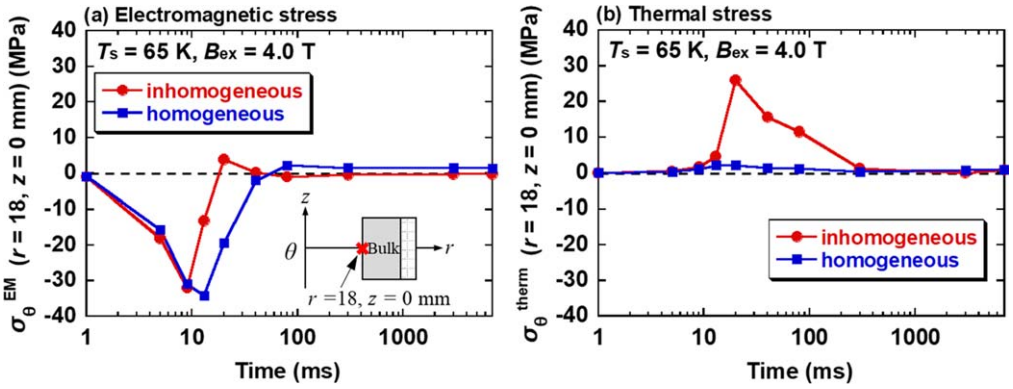

Figure 12. Time evolution of (a) the electromagnetic hoop stresses, $\sigma_\theta{}^{EM}(t)$, and (b) thermal hoop stress, $\sigma_\theta{}^{therm}(t)$, at the inner surface of the ring bulk (r = 18 mm, z = 0 mm) for B_{ex} = 4.0 T at T_s = 65 K for the homogeneous and inhomogeneous models.

and inner defects. To prevent a flux jump for the ring bulk, smaller and/or inner defects in bulk materials are desirable from the results of these numerical simulations.

A comment should be made here on the influence of the other parameters on the flux jump behavior. If the operating temperature decreases, the critical applied field, at which the flux jump takes place, should increase because of the increase in J_c. As for the influence of the rise time of the magnetic pulse on the flux jump, the critical applied field should increase with increasing rise time of the pulsed field because of the reduction in the temperature rise. Such influences on the flux jump will be investigated in the future.

3.5. Electromagnetic and thermal hoop stresses during PFM

The cause of the 'C-shaped profile' in the experimental results shown in figure 1 may result from the bulk fracture during PFM, in which the circulating supercurrent path was cut off, in addition to the being the origin of a flux jump. To clarify the possibility of fracture, the mechanical stress behavior was investigated during PFM using inhomogeneous model with outer notch, as shown in figure 4(b). Figure 12(a) shows time evolution of the electromagnetic hoop stress, $\sigma_\theta{}^{EM}(t)$, at the center of the inner surface of the ring bulk (r = 18 mm, z = 0 mm) for B_{ex} = 4.0 T at T_s = 65 K for the homogeneous and inhomogeneous models. $\sigma_\theta{}^{EM}(t)$ starts to increase negatively (compressive stress) and takes a peak value around t∼10 ms, at which the applied pulsed field takes a maximum. After that, $\sigma_\theta{}^{EM}(t)$ decreases and changes to a small positive value (tensile stress) for each case, which results from the change of the direction of the induced superconducting current. Similar numerical results are reported in [37–40]. The maximum tensile stress in the homogeneous and inhomogeneous models was +2 and +4 MPa, respectively, which are much smaller than the fracture strength of ∼70 MPa estimated by bending measurements [41–43]. On the other hand, the simulated maximum compressive stress of −30∼−40 MPa is about one order of magnitude larger than the maximum tensile stress. The fracture strength of the REBaCuO bulk for compressive stress was reported to be at least −200 MPa [44, 45]. These results suggest that it is highly unlikely that the bulk would fracture due to the electromagnetic stress during PFM.

Figure 12(b) shows the time evolution of the thermal hoop stress, $\sigma_\theta{}^{therm}(t)$, at the center of the inner surface of the ring bulk (r = 18 mm, z = 0 mm) for B_{ex} = 4.0 T at T_s = 65 K for the homogeneous and inhomogeneous models. The thermal hoop stress originates from the temperature distribution in the bulk reinforced by an Al alloy ring during PFM. The $\sigma_\theta{}^{therm}$ value in the homogenous model was very small due to a low temperature rise. On the other hand, in the inhomogeneous model, a maximum tensile hoop stress of +26 MPa was developed by the flux jump just after the peak of $B_{ex}(t)$ at t = 20 ms, which was smaller than the fracture strength of the bulk by bending tests [41–43]. These numerical simulation results of the electromagnetic and thermal hoop stresses suggest that the 'C-shaped trapped field profile' shown in figure 1 resulted from the flux jump rather than the bulk fracture. It should be noted that the sudden and large local temperature rise increasing by several decades may promote the flux jump. A bulk NMR magnet using stacked REBaCuO ring bulks has been developed, which was magnetized by FCM [4, 46, 47]. If such a bulk NMR magnet can be magnetized by PFM in the future, adequate measures to avoid such flux jumps may be necessary to mitigate an inhomogeneous trapped field profile.

4. Conclusion

We have investigated the electromagnetic and thermal properties of a REBaCuO ring bulk with an inhomogeneous critical current density, J_c, profile during pulsed field magnetization (PFM) using a numerical simulation and compared these to a bulk with a homogeneous J_c profile. The important results and conclusions of this study are summarized as follows.

(1) A notch was introduced in the bulk periphery, which was assumed as a crack existing in the actual bulk material. A sudden flux penetration (flux jump) took place through the notch area, and as a result, a large temperature rise also took place around this notch.

Consequently, the final trapped field profile was simulated to be 'C-shaped profile', which qualitatively reproduced our previous experimental results.

(2) The influence of the size and position of the notch on the occurrence of the flux jump was investigated. It was confirmed numerically that the larger and the outer notches, which simulates real imperfections, such as a crack, void or low J_c region, is easier to cause a flux jump.

(3) On the other hand, in the homogeneous model, no flux jump phenomenon was observed for all the cases studied. These results suggest that an imperfection in the bulk can be a possible starting point of a flux jump.

(4) The electromagnetic and thermal hoop stresses are simulated in the ring bulk during PFM. A compressive electromagnetic stress and a tensile thermal stress were observed around the peak of the pulsed magnetic field, both of which were lower than the experimentally measured fracture strength of the bulk material reported in the literature.

(5) We conclude that the experimentally observed 'C-shaped profile' results from the flux jump, rather than the bulk fracture. The size of the present notch is much larger than that of the realistic crack, which must be investigated in the future.

Acknowledgments

This research is partially supported by a 'Development of Systems and Technologies for Advanced Measurement and Analysis' from Japan Agency for Medical Research and Development, AMED and by JSPS KAKENHI Grant Nos. 15K04646 and 19K05240. M D Ainslie would like to acknowledge financial support from an Engineering and Physical Sciences Research Council (EPSRC) Early Career Fellowship, EP/P020313/1. All data are provided in full in the results section of this paper.

ORCID iDs

Tatsuya Hirano https://orcid.org/0000-0003-1658-914X
Hiroyuki Fujishiro https://orcid.org/0000-0003-1483-835X
Tomoyuki Naito https://orcid.org/0000-0001-7594-3466
Mark D Ainslie https://orcid.org/0000-0003-0466-3680

References

[1] Tomita M and Murakami M 2003 *Nature* **421** 517–20
[2] Durrell J H *et al* 2014 *Supercond. Sci. Technol.* **27** 082001
[3] Huang K-Y *et al* 2020 *Supercond. Sci. Technol.* **33** 02LT01
[4] Nakamura T, Tamada D, Yanagi Y, Itoh Y, Nemoto T, Utsumi H and Kose K 2015 *J. Magn. Reson.* **259** 68–75
[5] Yokoyama K, Oka T, Okada H, Fujine Y, Chiba A and Noto K 2003 *IEEE Trans. Appl. Supercond.* **13** 7711238
[6] Nishijima S, Mishima F, Tabata Y, Iseki H, Muragaki Y, Sasaki A and Saho N 2009 *IEEE Trans. Appl. Supercond.* **19** 10782044
[7] Zhou D, Izumi M, Miki M, Felder B, Ida T and Kitano M 2012 *Supercond. Sci. Technol.* **25** 103001
[8] Durrel J H, Ainslie M D, Zhou D, Vanderbemden P, Bradshaw T, Speller S, Filipenko M and Cardwell D A 2018 *Supercond. Sci. Technol.* **31** 103501
[9] Ren Y, Weinstein R, Liu J, Sawh R P and Foster C 1995 *Physica* C **251** 15–26
[10] Fuchs G, Schätzle P, Krabbes G, Gruß S, Verges P, Müller K-H, Fink J and Schultz L 2000 *Appl. Phys. Lett.* **76** 2107–9
[11] Tomita M and Murakami M 2001 *Physica C* **354** 358–62
[12] Nariki S, Sakai N and Murakami M 2004 *Supercond. Sci. Technol.* **18** S126
[13] Fujishiro H, Ainslie M D, Takahashi K, Naito T, Yanagi Y, Itoh Y and Nakamura T 2017 *Supercond. Sci. Technol.* **30** 085008
[14] Takahashi K, Fujishiro H, Naito T, Yanagi Y, Itoh Y and Nakamura T 2017 *Supercond. Sci. Technol.* **30** 115006
[15] Fujishiro H, Naito T, Yanagi Y, Itoh Y and Nakamura T 2019 *Supercond. Sci. Technol.* **32** 065001
[16] Fujishiro H, Naito T and Awaji S 2019 *Supercond. Sci. Technol.* **32** 045005
[17] Ainslie M D, Huang K Y, Fujishiro H, Chaddock J, Takahashi K, Namba S, Cardwell D A and Durrell J H 2019 *Supercond. Sci. Technol.* **32** 034002
[18] Johansen T H 1999 *Phys. Rev.* B **60** 9690
[19] Johansen T H, Wang C, Chen Q Y and Chu W-K 2000 *J. Appl. Phys.* **88** 2730–3
[20] Johansen T H 2000 *Supercond. Sci. Technol.* **13** R121
[21] Mochizuki H, Fujishiro H, Naito T, Itoh Y, Yanagi Y and Nakamura T 2016 *IEEE Trans. Appl. Supercond.* **26** 6800205
[22] Korotkov V S, Krasnoperov E P and Kartamyshev A A 2016 *J. Phys.: Conf. Ser.* **695** 012007
[23] Korotkov V S, Krasnoperov E P and Kartamyshev A A 2017 *Supercond. Sci. Technol.* **30** 095004
[24] Weinstein R, Parks D, Sawh R-P, Davey K and Carpenter K 2015 *IEEE Trans. Appl. Supercond.* **25** 6601106
[25] Weinstein R, Parks D, Sawh R-P, Carpenter K and Davey K 2016 *J. Appl. Phys.* **119** 133906
[26] Zhou D, Ainslie M D, Shi Y, Dennis A R, Huang K, Hull J R, Cardwell D A and Durrell J H 2017 *Appl. Phys. Lett.* **110** 062601
[27] Zhou D, Ainslie M D, Srpčič J, Huang K-Y, Shi Y-H, Dennis A R, Cardwell D A, Durrell J H, Boll M and Filipenko M 2018 *Supercond. Sci. Technol.* **31** 105005
[28] Ainslie M D, Zhou D, Fujishiro H, Takahashi K, Shi Y-H and Durrell J H 2016 *Supercond. Sci. Technol.* **29** 124004
[29] Takahashi K, Ainslie M D, Fujishiro H, Naito T, Shi Y-H and Cardwell D A 2017 *Physica* C **536** 1–10
[30] Fujishiro H and Naito T 2010 *Supercond. Sci. Technol.* **23** 105021
[31] Ainslie M D and Fujishiro H 2015 *Supercond. Sci. Technol.* **28** 053002
[32] Jirsa M, Pust L, Dlouhy D and Koblischka M R 1997 *Phys. Rev.* B **55** 3276
[33] Kii T *et al* 2012 *IEEE Trans. Appl. Supercond.* **22** 4100904
[34] Ainslie M D, Fujishiro H, Mochizuki H, Takahashi K, Shi Y-H, Namburi D K, Zou J, Zhou D, Dennis A R and Cardwell D A 2016 *Supercond. Sci. Technol.* **29** 074003
[35] Hirano T, Takahashi K, Shimoyashiki F, Fujishiro H, Naito T and Ainslie M D 2019 *IEEE Trans. Appl. Supercond.* **29** 8000705
[36] Ainslie M D, Fujishiro H, Ujiie T, Zhou J, Dennis A R, Shi Y-H and Cardwell D A 2014 *Supercond. Sci. Technol.* **27** 065008

[37] Yang X, Li X, He Y, Wang X and Xu B 2017 *Physica* C **535** 1–8
[38] Wu H, Yong H and Zhou Y 2018 *Supercond. Sci. Technol.* **31** 045008
[39] Shimoyashiki F, Fujishiro H, Hirano T, Naito T and Ainslie M D 2019 *14th European Conf. on Applied Superconductivity (EUCAS2019)*
[40] Hirano T, Fujishiro H, Naito T and Ainslie M D 2019 *14th European Conf. on Applied Superconductivity (EUCAS2019)*
[41] Murakami A, Miyata H, Hashimoto R, Katagiri K and Iwamoto A 2009 *IEEE Trans. Appl. Supercond.* **19** 2995–8
[42] Murakami A, Miyata H, Hashimoto R, Katagiri K and Iwamoto A 2008 *Physica* C **468** 1395–8
[43] Fujimoto H, Murakami A, Teshima H and Morita M 2013 *Cryogenics* **57** 6–11
[44] Kan R, Katagiri K, Murakami A, Kasaba K, Shoji Y, Noto K, Sakai N and Murakami M 2004 *IEEE Trans. Appl. Supercond.* **14** 8132078
[45] Murakami A, Katagiri K, Kan R, Miyata H, Shoji Y, Noto K, Iwamoto A and Mito T 2005 *Physica* C **426–431** 644–8
[46] Nakamura T, Itoh Y, Yoshikawa M, Oka T and Uzawa J 2007 *Concepts Magn. Reson.* B **31B** 65–70
[47] Ogawa K, Nakamura T, Terada Y, Kose K and Haishi T 2011 *Appl. Phys. Lett.* **98** 234101